Tapped Marchand Baluns for Matching Applications

Wael M. Fathelbab, *Senior Member, IEEE*, and Michael B. Steer, *Fellow, IEEE*

Abstract—**Compact three-terminal structures with integrated matching and balun functionality are presented. The structures are in the form of tapped Marchand baluns and possess prescribed immittance profiles at either their single-ended or balanced ports. These prescribed profiles are important in ensuring stability of active circuits. Tapping the balanced resonators of the baluns enables the realization of an extremely wide range of load-to-source impedance or admittance ratios at no increase in overall size. Designs and implementations of two tapped Marchand baluns with octave bandwidths centered at 500 MHz are presented.**

Index Terms—**Doubly/singly terminated prototypes, load-to-source immittance ratios, Marchand balun, matching networks, network synthesis, radio-frequency integrated circuits (RFICs), stability.**

I. INTRODUCTION

BALUNS [1] are key components of any radio-frequency (RF) and microwave communication system. They are used in balanced circuits, such as double-balanced mixers, push–pull amplifiers, and frequency doublers [2]. Another application of a balun is in a system using an RF integrated circuit (RFIC), where a balun transforms the differential outputs of an RFIC to unbalanced microwave circuitry. There are many types of baluns [3]–[5], with the Marchand balun [1], [2], [6]–[13] being the most popular at microwave frequencies, as it can be conveniently realized in planar or coaxial forms [1].

Generally, subsystems with active devices require matching networks which, as well as providing optimum transfer of power within an operating band, often determine the stability of the subsystem by their out-of-band characteristics. Essentially, a matching network must extract maximum power from the source for transfer to the load, but must also present the source with a specific immittance profile both in and out of its operating band. For example, the impedance level of a matching network connected to the output of a power amplifier approximating a current source must drop to a low level in the out-of-band region to ensure device stability. These design criteria influence the requirements imposed on the matching network, necessitating that its design be based on a singly terminated [14]–[17] rather than a doubly terminated network [9]. In the case of a singly terminated matching network, the real part of its input immittance function becomes the design parameter and, hence, is tailored appropriately to suit the characteristics of the source.
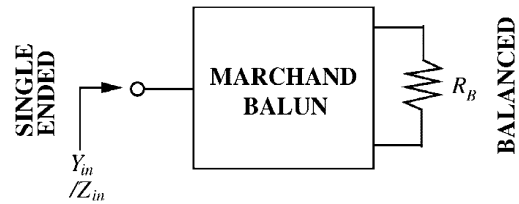
Fig. 1. Marchand balun.

This paper presents structures that combine the functionality of baluns and matching networks. The structures are derived from several filter prototypes [9] that can be realized in the form of Marchand baluns. The baluns represent a solution to the problem of matching between terminals of extreme impedance (or admittance) values without using elements of extreme characteristic impedances in the balun structures. This is by virtue of tapping the balanced resonators of the baluns, thus allowing a wide range of load-to-source immittance ratios to be realized.

The presentation here begins in Section II by highlighting the difference in design objective between doubly and singly terminated networks. Then, Section III proposes a method of scaling the balanced load of a balun to specific values. Finally, Section IV presents the synthesis and implementation of two tapped baluns and reports their measured performances. Size miniaturization and specific load-to-source immittance ratios are achieved.

II. DOUBLY AND SINGLY TERMINATED MATCHING NETWORKS

The fundamental difference between doubly and singly terminated matching networks concerns the design parameter that is synthesized to satisfy an electrical specification.

A. Doubly Terminated Network

A doubly terminated network attempts to achieve a constant return-loss level at its terminals over a specified passband. By referring to Fig. 1, the design focus is the input reflection coefficient

$$\Gamma_{\text{in}} = \frac{Z_{\text{in}} - R_S}{Z_{\text{in}} + R_S} \tag{1}$$

for an impedance-based network where R_S is the source impedance. The input reflection coefficient can also be expressed as

$$\Gamma_{\text{in}} = \frac{Y_s - Y_{\text{in}}}{Y_s + Y_{\text{in}}} \tag{2}$$

for an admittance-based network where $Y_S(= 1/R_s)$ is the source admittance. In a lossless system, the transmission char-

acteristic is then related to the reflection coefficient through the well-known relationship

$$|S_{21}|^2 = 1 - |\Gamma_{\text{in}}|^2 \qquad (3)$$

implying that delivery of the power from source to load is controlled by controlling the magnitude of the input reflection coefficient.

B. Singly Terminated Network

An ideal impedance-based singly terminated network is driven by a pure current source and presents a constant-impedance level to its driving source over its operating band. Upon analysis, it can be shown that the transmission coefficient of a singly terminated network is actually equal to the real part of its input impedance [16], [17]. This is expressed as

$$|S_{21}|^2 = \text{Re}(Z_{\text{in}}). \qquad (4)$$

Also, for an admittance-based network driven by a pure voltage source, the transmission characteristic is

$$|S_{21}|^2 = \text{Re}(Y_{\text{in}}). \qquad (5)$$

It is now evident from (3)–(5) that the transfer of power from the source to load is different in the two cases.

C. Balun Example

To demonstrate the points described above, we investigate the performance of a third-order class-A Marchand balun [9] designed from doubly and singly terminated prototypes.

Fig. 2(a) presents plots of the real part of the balun's input admittance function at the single-ended port. Here, it is shown how the characteristic of the real part changes as the return-loss level is varied from 10 to 20 dB. As expected, the passband ripple decreases as the return loss improves. However, it is also seen, from Fig. 2(a), that the real part peaks at frequencies outside the passband (which is defined by the vertical dotted lines) as the return loss improves, thus resulting in an uncontrolled increase in bandwidth. In other words, in order to improve the in-band ripple of the input admittance level, the skirt selectivity must be degraded. In almost every application, the skirt selectivity of a matching network is equally as important as the quality of the in-band match and has direct influence on the overall system performance.

Now, the same type of balun is synthesized on singly terminated basis [see the characteristic in Fig. 2(b)]. Here, we see that the transition from passband to stopband is much faster than that of any of the functions presented in Fig. 2(a). In addition, there is a more controlled in-band ripple variation. The function depicted in Fig. 2(b) is Chebyshev, which is well known for its optimum performance in terms of trading off passband ripple and skirt selectivity [16].

Thus, based on the proceeding comparison, it is possible to conclude that a singly terminated balun integrated as a matching
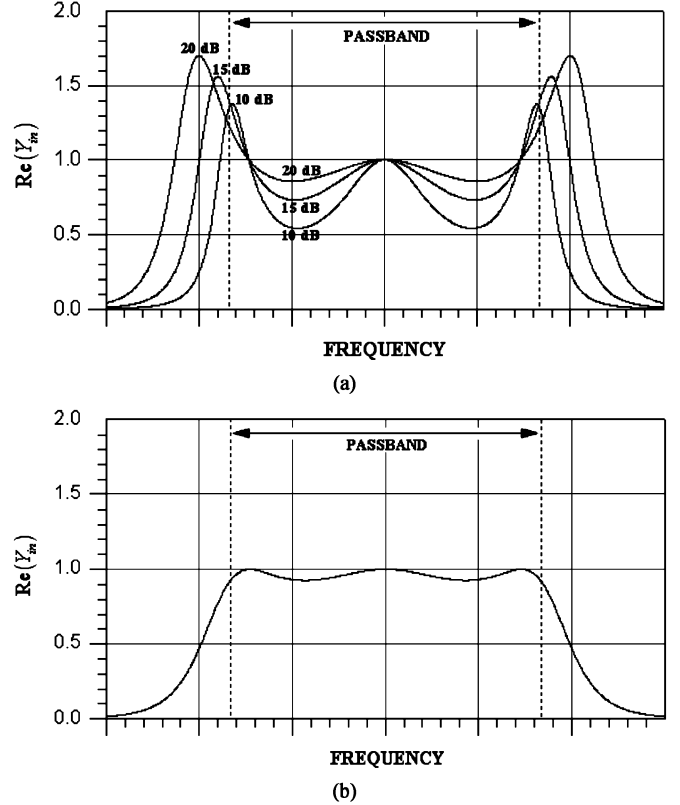
Fig. 2. Input admittance of class-A Marchand balun normalized to a 1-Ω system. (a) Real part of the input admittance of a balun designed from a doubly terminated prototype for various single-ended return-loss level. (b) The same balun designed utilizing a singly terminated prototype with a specific passband ripple.

TABLE I
TYPE OF PARAMETER SYNTHESIZED FOR EACH CLASS OF BALUNS.
(S IS THE RICHARDS TRANSFORMATION)

Prototype classes [9]	Distribution of Zeros	Type of parameter realized at single-ended port	Type of parameter realized at balanced ports
A	2 zeros at $S=0$ 2 zeros at $S=\infty$ 2 zeros at $S=1$	$\text{Re}(Y_{in})$	$\text{Re}(Z_{in})$
C1	2 zeros at $S=0$ 1 zero at $S=\infty$ 1 zero at $S=1$	$\text{Re}(Y_{in})$	$\text{Re}(Z_{in})$
C2	1 zero at $S=0$ 2 zeros at $S=\infty$ 1 zero at $S=1$	$\text{Re}(Z_{in})$	$\text{Re}(Z_{in})$
B	2 zeros at $S=0$ 2 zeros at $S=\infty$	$\text{Re}(Z_{in})$	$\text{Re}(Z_{in})$

network in a subsystem configuration will extract maximum available power from its source and will possess the desired out-of-band characteristics for stability requirements of active circuits. Table I summarizes the type of parameter that is synthesized at either port with reference to the sets of transmission zeros used to design baluns in [9].

III. TAPPING THE BALANCED RESONATORS OF THE BALUN

This section shows that the balun of Fig. 3(a) [9] can be designed for specific load-to-source immittance ratios. The equiv-
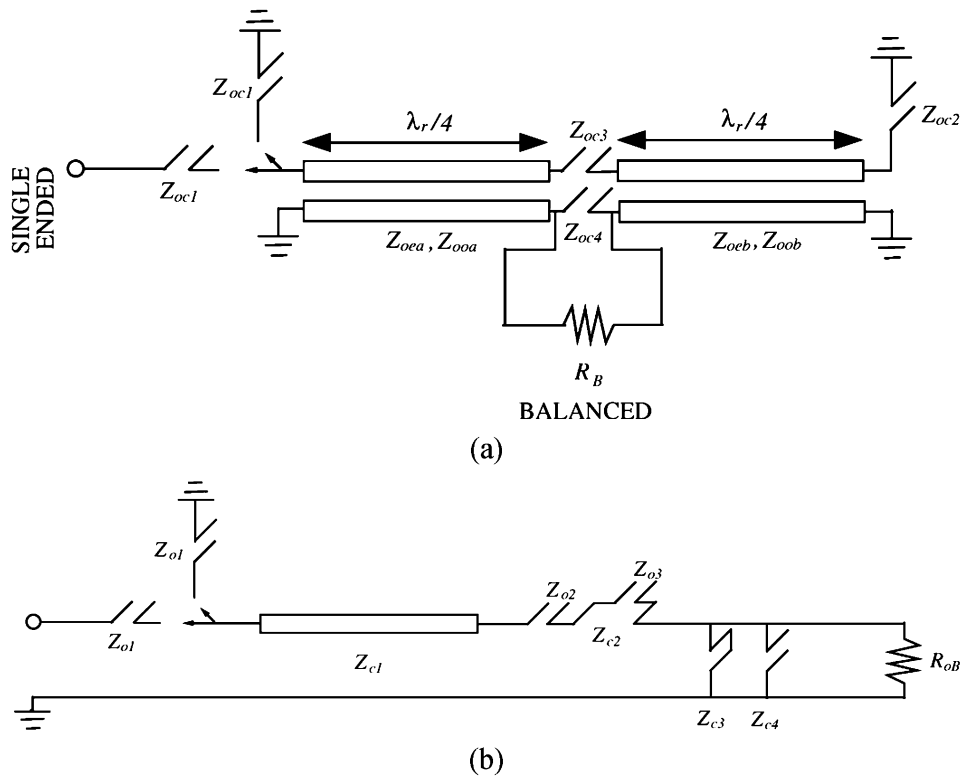
Fig. 3. Bandpass Marchand balun with a balanced load impedance R_B from [9]. (a) Its physical layout. (b) Its corresponding S-plane bandpass prototype.

alent prototype of this balun illustrated in Fig. 3(b) can be synthesized for different commensurate frequencies, f_r. The commensurate frequency determines the electrical lengths of the transmission lines forming the balun and, thus, the larger the value of f_r, the smaller the size of the resulting balun structure. In addition to fixing the overall size of the balun, the choice of the commensurate frequency also impacts the values of the immittances terminating the balun. In general, the inherent values of the load and source immittances of a Marchand balun are functions of the passband ripple, operating bandwidth, and the commensurate frequency. An example of a synthesized balun with an octave bandwidth centered at 500 MHz is shown in Fig. 4. It is seen that the inherent values of the single-ended and balanced impedances drop as f_r increases from 5 to 20 GHz. In other words, miniaturizing such a structure has an impact on its terminal impedances. It is also observed that the inherent balanced-to-single-ended impedance ratios and the modal impedances in the two cases remain practically unaffected for different values of f_r. We will now focus on tapping the balanced resonators of the balun to achieve a wide range of balanced-to-single-ended immittance ratios.

The detailed analysis of the generalized Marchand balun of [9] demonstrated that the balanced load is always much higher in value than the single-ended source impedance. It is common practice to scale down the balanced load impedance by using a pair of quarter-wavelength transmission lines. For example, see [9, Fig. 10(f)]. While this is normally an acceptable technique, the pair of transmission lines drastically increased the overall size of the balun. Note that these matching lines resonated at the passband center frequency f_o while the balun structure com-

prised transmission lines that resonated at the commensurate frequency f_r, where $f_r > f_o$. This situation is undesirable in circumstances where size reduction is the primary objective. To overcome this drawback and to simultaneously achieve a specific load-to-source immittance ratio, we propose tapping the balanced resonators of the balun. It is common practice to alter the system impedance at either or both ports of a microwave filter (such as Combline [18]) to yield a realizable circuit. Consequently, tapping the resonators at the scaled node(s) of the filter matches to the desired system impedance with the advantage of no added hardware. This approach has potential usage in designing Marchand baluns.

To begin the description of the tapped balun design, consider Fig. 5(a), which illustrates the basic output subsection of a bandpass Marchand balun. The subsection consists of a short-circuited stub, representing the balanced resonators, and an open-circuited stub connected to the balanced load R_B. To scale the load impedance from R_B to $R_D(R_D < R_B)$, an ideal $1 : X$ transformer $(X = \sqrt{R_D/R_B})$ is inserted at the output, as shown in Fig. 5(a). If the balun is designed such that the virtual ground plane bisects the subcircuit right in the center, then it is possible to exactly represent the subcircuit of Fig. 5(a) by that of Fig. 5(b). The subcircuit of Fig. 5(b) (excluding the open-circuited stub) can then be approximated by that of Fig. 5(c). Examination of the subcircuit of Fig. 5(c) reveals that the total length of the balanced resonators is still equal to l_r, but now the short-circuited stubs of length l_1 represent the parts of each resonator seen by each half of the scaled balanced load to the virtual ground. Also, the existence of the lumped capacitor C_o is required for fine-tuning purposes.
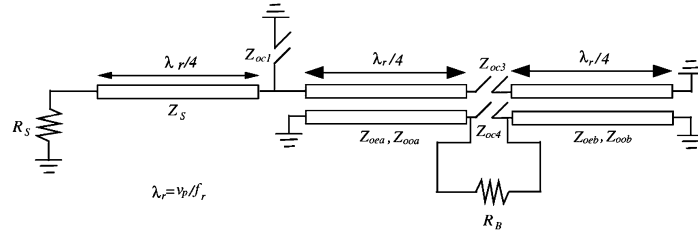
f_r (GHz)	Z_s (Ω)	Z_{oc1} (Ω)	Z_{oc3} (Ω)	Z_{oc4} (Ω)	$Z_{oea} = Z_{oeb}$ (Ω)	$Z_{ooa} = Z_{oob}$ (Ω)	R_s (Ω)	R_B (Ω)	R_B/R_S
5	47.55	1.56	3.117	4.744	164.946	58.253	6.166	59.988	9.728
10	48.028	0.385	0.787	1.184	166.842	59.421	3.127	30.567	9.775
20	48.148	0.095	0.197	0.294	167.502	59.827	1.569	15.373	9.797

(b)

f_r (GHz)	Z_s (Ω)	Z_{oc1} (Ω)	Z_{oc3} (Ω)	Z_{oc4} (Ω)	$Z_{oea} = Z_{oeb}$ (Ω)	$Z_{ooa} = Z_{oob}$ (Ω)	R_s (Ω)	R_B (Ω)	R_B/R_S
5	35.695	0.985	3.345	5.245	189.411	50.789	2.748	39.173	14.255
10	36.257	0.245	0.845	1.310	191.724	52.069	1.396	19.988	14.318
20	36.399	0.061	0.211	0.326	192.152	52.307	0.701	10.035	14.315

(c)

Fig. 4. (a) Electrical layout of a class-A balun with an octave bandwidth centered at 500 MHz. (b) Element values for a prescribed impedance function at the balanced ports with a passband ripple of 0.5 dB. (c) Element values for a prescribed admittance function at the single-ended port with a passband ripple of 0.5 dB.

For a balun realizing a prescribed immittance function at the single-ended port, the following approximation is valid for passband bandwidths up to an octave. At the center frequency f_o, the impedance Z_T in Fig. 5(b) is

$$Z_T = \Re_T + j\Im_T \tag{6}$$

where

$$\Re_T = \frac{2R_D^2}{R_B \left(\frac{4R_D^2}{Z_{sc}^2 (\tan(\beta l_r))^2} + \frac{4R_D^2}{R_B^2} \right)} \tag{7}$$

and

$$\Im_T = \frac{2R_D^2}{Z_{sc}(\tan(\beta l_r)) \left(\frac{4R_D^2}{Z_{sc}^2 (\tan(\beta l_r))^2} + \frac{4R_D^2}{R_B^2} \right)}. \tag{8}$$

Now, the ABCD matrix of half of the circuit of Fig. 5(c) (without including the load impedance) can be derived based on the following matrix manipulations:

$$\begin{bmatrix} 1 & 0 \\ j(2\pi f)C_o & 1 \end{bmatrix}$$
$$\times \begin{bmatrix} \cos(\beta(l_r - l_1)) & j\left(\frac{Z_{sc}}{2}\right)\sin(\beta(l_r - l_1)) \\ j\left(\frac{2}{Z_{sc}}\right)\sin(\beta(l_r - l_1)) & \cos(\beta(l_r - l_1)) \end{bmatrix}$$
$$\times \begin{bmatrix} 1 & 0 \\ j\left(\frac{Z_{sc}}{2}\right)\tan(\beta l_1) & 1 \end{bmatrix} = \begin{bmatrix} A & B \\ C & D \end{bmatrix}. \tag{9}$$

Using (9), the input impedance Z_t is evaluated at f_o to give

$$Z_t = \frac{A(R_D/2) + B}{C(R_D/2) + D} = \Re_t + j\Im_t. \tag{10}$$

In (7)–(9), $\beta(= ((2\pi/\lambda)) = ((2\pi f)/(v_p)))$ is the propagation constant and v_p is the phase velocity in the transmission media. The real and imaginary parts of (6) and (10) may now be equated and solved simultaneously for the two unknowns l_1 and C_o. It should be appreciated, however, that there is a limit as to how much the balanced load impedance can be lowered from R_B to R_D using the tapping approach. For example, forcing R_D to be a very low value will likely degrade the ripple level of the real part of the input immittance at the single-ended port. In general, the approximation is increasingly valid as R_D approaches $R_B/2$.

The above procedure can also be used to scale the balanced load of a balun realizing a prescribed immittance function at its balanced ports. In this case, it is more appropriate to approximate the subcircuit of Fig. 5(b) by that of Fig. 5(d) in a similar fashion as was just described. The process of load scaling will be demonstrated as part of the examples to be discussed in Section IV.

IV. NUMERICAL SYNTHESIS EXAMPLES AND BALUN IMPLEMENTATIONS

The general form of the characteristic polynomial of an S-plane highpass network comprising m open- or short-circuited stubs and n quarter-wavelength transmission lines is [19], [20]

$$k(S) = \sqrt{\cos\left(m\cos^{-1}\left(\frac{S_c}{S}\right) + n\cos^{-1}\left(\sqrt{\frac{1 - S_c^2}{1 - S^2}}\right) \right)} \tag{11}$$

where S is the Richards transformation defined as $\tan((\pi/2)(f)/(f_r))$, where f and S are the real and complex frequency variables, respectively, and f_r is the commensurate

$$l_r = \lambda_r/4 = \left(v_p/f_r\right)/4; \quad X = \sqrt{R_D/R_B}$$

(a)

(b)

(c)

(d)
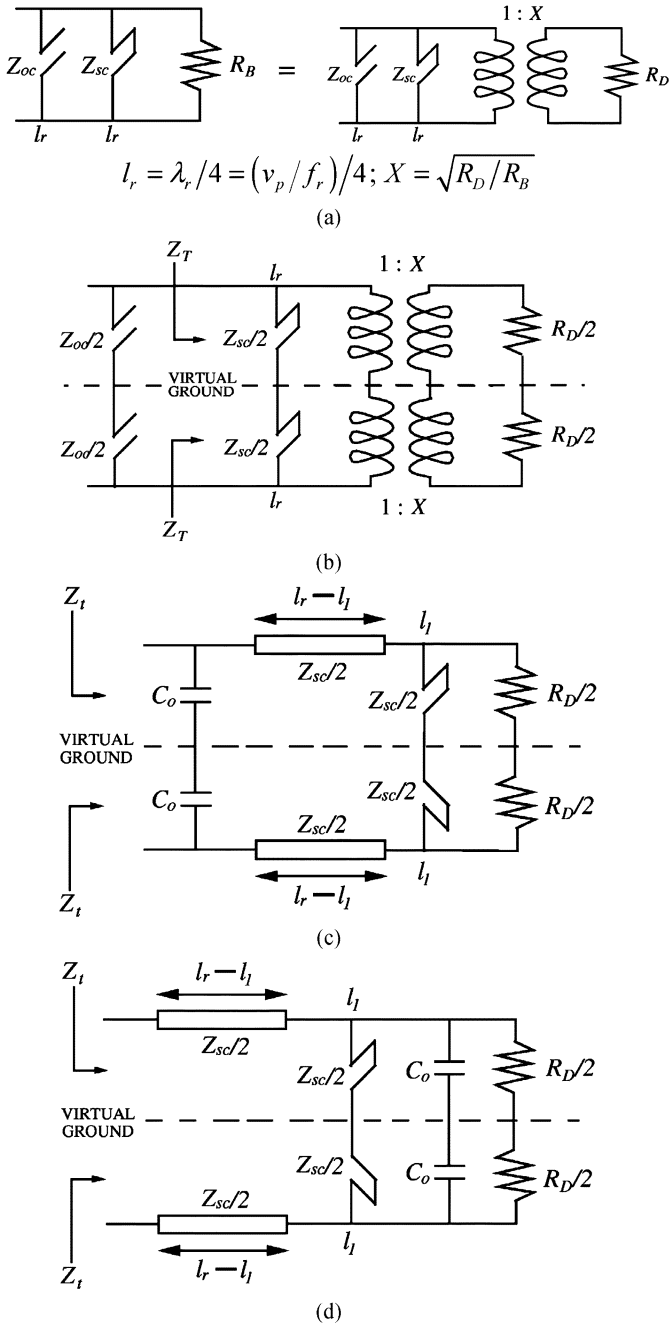
Fig. 5. Balanced resonator tapping. (a) Typical output section of a bandpass balun prototype after scaling its balanced load using an ideal transformer. (b) Identification of the virtual ground plane. (c) and (d) Balanced resonators after tapping.

frequency at which the transmission lines of the prototype are equal to a quarter-wavelength long. For the prototypes to be synthesized, we have $m = 2$ and $n = 1$, i.e., the prototypes have a pair of zeros at dc and a single zero at $S = 1$. For an octave bandwidth, (11) becomes

$$k(S) = \frac{-S^2\left(2S_c^2 + S_c^2\sqrt{1 - S_c^2}\right) + \left(2\sqrt{1 - S_c^2} + 2\right)}{S^3\left(S_c^3\sqrt{1 - \frac{1}{S^2}}\right)}$$

(12)

with S_c equal to $j0.57735$. The FR4 substrate utilized for the fabrication of the baluns had a thickness of 1.57 mm, a relative dielectric constant of 4.7, and a loss tangent of 0.016.

A. A Balun With Prescribed Admittance Function at the Single-Ended Port

A class-A balun is required to have a prescribed immittance function at its single-ended port with a passband ripple ε of 0.508 (i.e., $10\log_{10}(1/(1 + \varepsilon^2)) = 1$ dB) centered at 500 MHz. According to Table I, we will be dealing with an admittance function. The balun is also required to transform a single-ended source impedance of 7 Ω to a balanced load of 100 Ω. A typical situation that requires this type of balun is in the matching stage between the output of a low-impedance power amplifier and a balanced circuit such as an antenna.

Using (12), the real part of the input admittance is derived from

$$\mathrm{Re}(Y_{\mathrm{in}}(S)) = \frac{1}{1 + \varepsilon^2|k(S)|^2} = |S_{21}(S)|^2.$$

(13)

Partial fraction expansion of (13) is then applied, after which the input admittance is extracted with the knowledge of the relationship [16], [17]

$$\mathrm{Re}(Y_{\mathrm{in}}(S)) = 0.5 \times \{Y_{\mathrm{in}}(S) + Y_{\mathrm{in}}(-S)\}.$$

(14)

This gives

$$Y_{\mathrm{in}}(S) = \frac{(0.1662867861 + j0.3615083714)}{(S + 0.4719034609 - j1.681902406)}$$
$$+ \frac{(0.1662867847 - j0.361508366)}{(S + 0.4719034609 + j1.681902406)}$$
$$- \frac{2.438018122}{(S + 3.734004591)} + 1.$$

(15)

Note that all the poles of the input admittance of (15) are located in the left-hand side of the S-plane to ensure that the input impedance is positive real. The above function is then synthesized to obtain an S-plane singly terminated prototype with element values as shown in Fig. 6(a). It is worth mentioning that each S-plane capacitor and inductor of Fig. 6(a) become an open- and a short-circuited stub in the f-plane with a characteristic impedance of $1/C$ and L, respectively. The system impedance of the prototype is then raised from 1 to 7 Ω, after which the half-angle [21] and relevant Kuroda transformations are applied, resulting in a transformed bandpass prototype. This leads to the f-plane prototype of Fig. 6(b). The element values of the circuit of Fig. 3(b) may now be obtained from the circuit of Fig. 6(b). They are as follows:

$$Z_{o1} = 28.023 \ \Omega$$
$$Z_{c1} = 77.777 \ \Omega$$
$$Z_{o2} = 0$$
$$Z_{c2} = 78.287 \ \Omega$$
$$Z_{o3} = 502.364 \ \Omega$$
$$Z_{c3} = 70.025 \ \Omega = Z_{c4}$$
$$R_{oB} = 60.669 \ \Omega.$$

(16)

(a)

(b)

(c)

(d)

(e)
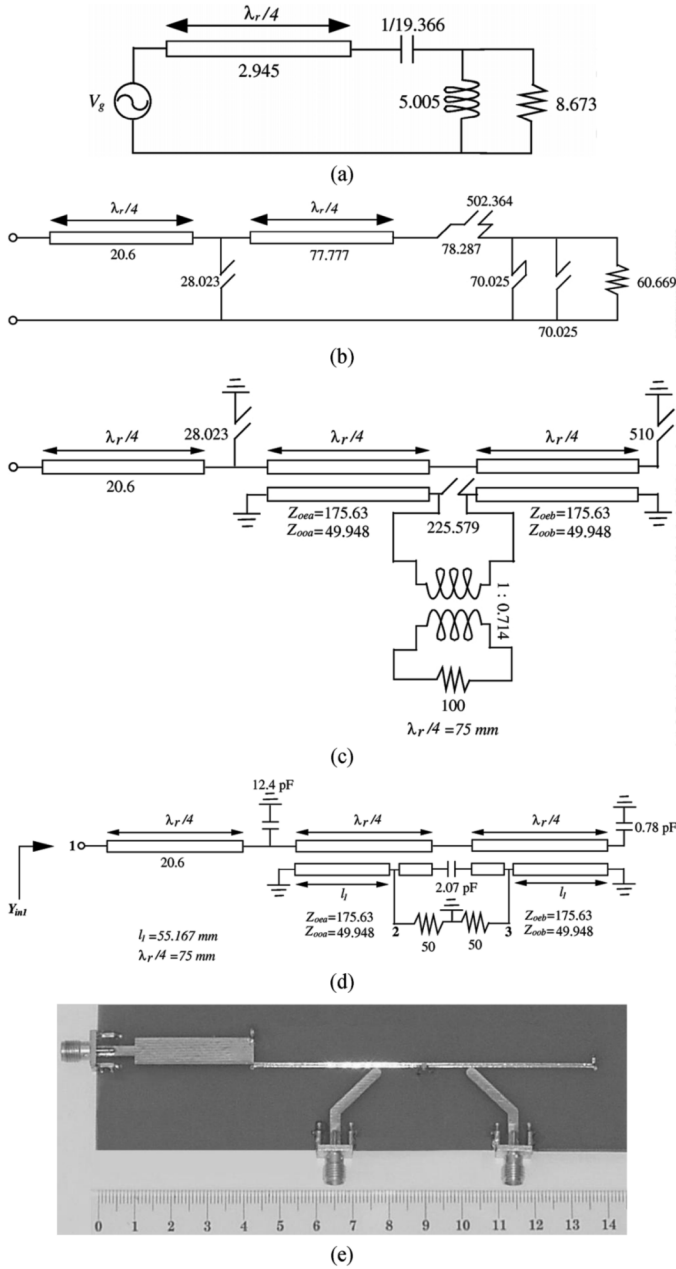
Fig. 6. Class-A balun with prescribed admittance function at the single-ended port. (a) S-plane singly terminated prototype. (b) Admittance-scaled and circuit-transformed f-plane prototype. (c) Electrical layout depicting the modal impedances of the coupled lines. (d) Layout with tapped resonators. (e) Fabricated balun.

Substituting (16) into (20)–(22), the parameters of the balun of Fig. 6(c) can be derived using (23)–(26). Fig. 6(c) depicts a load impedance of $100\,\Omega$ after the inclusion of a 1:0.714 transformer. This implies that the balun has an inherent balanced-to-single-ended impedance ratio of

$$\frac{R_{\mathrm{D}}}{R_{\mathrm{S}}} = \frac{195.879}{7} = 27. \qquad (17)$$

From Fig. 6(c), we see that the pairs of coupled lines of the balun possess identical modal impedances. This is by virtue of the appropriate sequence of circuit transformations applied to the initial prototype of Fig. 6(a). Due to this, the balanced load and
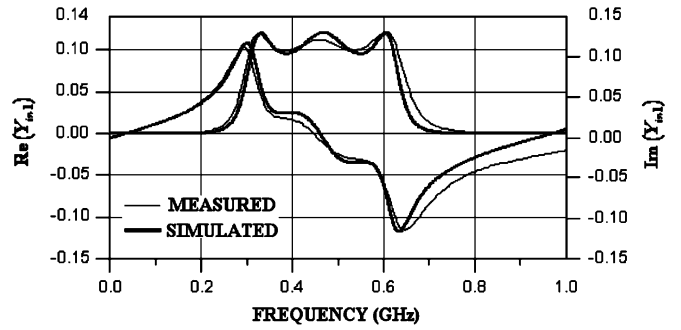
Fig. 7. Measured characteristics of the fabricated balun of Fig. 6(e).

the output shunt stubs are symmetrically bisected by a virtual ground plane right in the center. Thus, the resonator tapping approach discussed in Section III can be implemented. For this balun, the elements of the output subsection [corresponding to Fig. 5(a)] are

$$Z_{\mathrm{oc}} = 225.579\,\Omega$$
$$Z_{\mathrm{sc}} = 225.579\,\Omega$$
$$R_B = 195.879\,\Omega$$
$$R_D = 100\,\Omega$$
$$l_r = 75\text{ mm}$$
$$X = 0.714 \qquad (18)$$

which, upon solving (6) and (10), yields the tapping height and the value of the capacitor as follows:

$$l_1 = 55.787\text{ mm} \quad C_o = 1.313\text{ pF}. \qquad (19)$$

At this stage, the open-circuited stubs in the balun structure of Fig. 6(c) are approximated by lumped capacitors leading to the electrical layout of Fig. 6(d). Subsequently, the electrical layout of the balun is then converted into a physical layout using ADS [22] and then fabricated as shown in Fig. 6(e).

For practical purposes, additional sections of 50-Ω lines interconnecting the SMA connectors to the actual balun ports were added, as shown in Fig. 6(e). The extra transmission lines at the balanced ports have no effect on the measured response at the single-ended port; however, the delay introduced between the SMA connector and the actual single-ended port of the balun must be deembedded in order to accurately measure the input admittance. A pair of 50-Ω loads was connected at the balanced ports and the single-ended port of the balun connected to a Tektronix Digital Sampling Oscilloscope with a TDR/sampling head SD-24. The measured time delay t due to the transmission-line section at the single-ended port was 82.5 ps.

The measured performance of the balun is shown in Fig. 7. It is observed that the center frequency of the passband has been offset by 6.6% and is now centered at about 467 MHz. This offset is due to the unaccounted parasitic inductances of the via holes and can be corrected by slightly shortening the transmission line resonators of the balun. However, since this implementation is only for demonstration purposes, the measured performance of the balun is compared with the simulated characteristic of the final circuit of Fig. 6(d) but scaled down
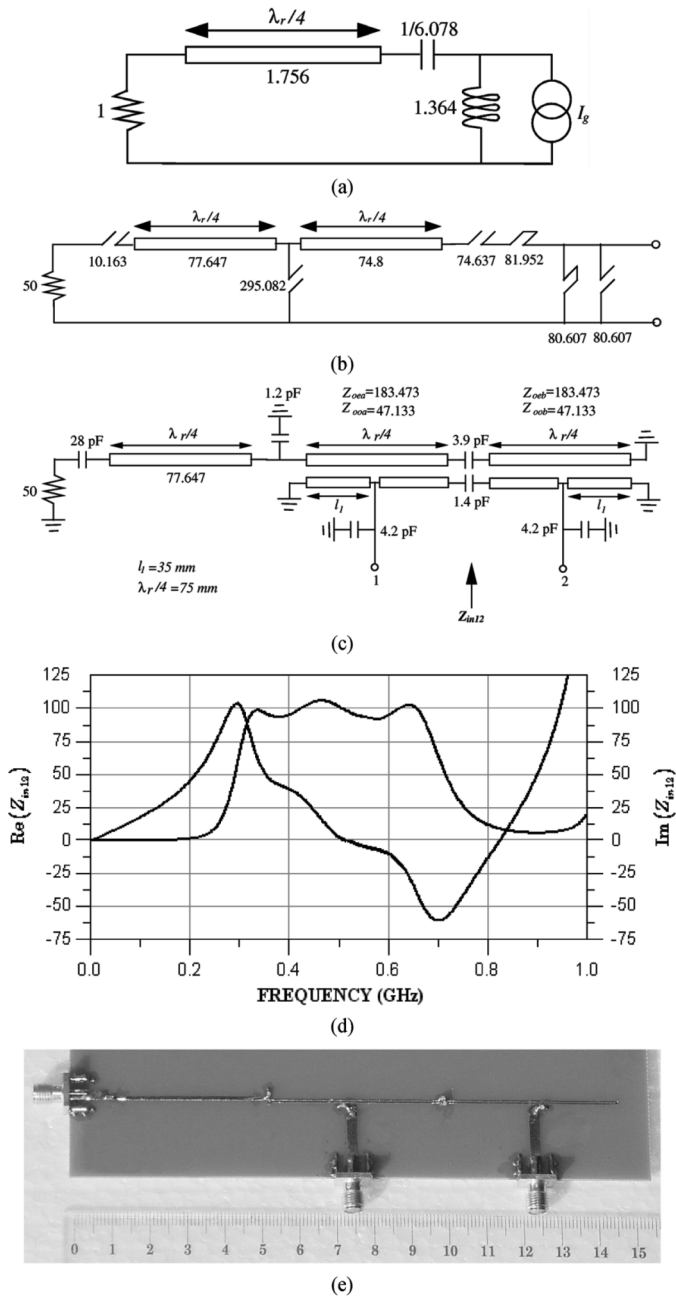
Fig. 8. Class-A balun with prescribed impedance function at the balanced ports. (a) S-plane singly terminated prototype. (b) Impedance-scaled and circuit-transformed f-plane prototype. (c) Electrical layout with tapped resonators depicting the modal impedances of the coupled-lines. (d) Simulation of the differential impedance between Ports 1 and 2. (e) Fabricated balun.

Fig. 9. Measured characteristics of the balun of Fig. 8(e). (a) and (b) Real and imaginary parts of the driving point impedances seen to ground at each balanced port with the other terminated in a 50-Ω load.

by 33 MHz. The correspondence is excellent. Next, the amplitude and phase imbalances were characterized. This was done using a 50-Ω network analyzer, notwithstanding the fact that the measured single-ended port impedance of the balun is 7 Ω. The measured amplitude and phase imbalances were found to be less than 0.2 dB and 1°, respectively.

B. Balun With Prescribed Impedance Function at the Balanced Ports

Here, we demonstrate that it is possible to synthesize a prescribed immittance function at the balanced ports of a Marc-

hand balun. The class-A balun of the previous subsection is required to transform a balanced source impedance of 100 Ω to a single-ended load of 50 Ω over the same frequency band, but with a ripple ε of 0.349 (0.5 dB). According to Table I, the structure will realize an impedance function. A typical application that requires this type of balun is in the matching stage between the differential outputs of an RFIC feeding a single-ended circuit such as a filter.

The real part of the balanced impedance function was constructed in an identical fashion as done previously using (12)–(14) but on impedance basis. The synthesized S-plane prototype is shown in Fig. 8(a). The prototype is then scaled up in impedance such that a 50-Ω load results at the single-ended port, resulting in the f-plane prototype of Fig. 8(b). Going through identical steps as discussed in Section III, the tapped balun of Fig. 8(c) results with its simulated differential impedance depicted in Fig. 8(d). The fabricated balun is shown in Fig. 8(e).

Balanced operation of the balun was tested by measuring the real and imaginary parts of the impedance function to ground at Port 1 of Fig. 8(c) with Port 2 terminated to ground in a 50-Ω load. Similar measurement at Port 2 with Port 1 terminated with 50 Ω was also performed. The deembedded measured characteristics are shown in Fig. 9 together with the simulation. Very good agreement between the simulated and measured results is observed.

V. CONCLUSION

Singly terminated prototypes were used to derive new immittance-transforming Marchand baluns suitable for matching pur-

poses. This led to miniaturized lumped-distributed baluns realizing specific immittance profiles at either their single-ended or balanced ports. Stability of active devices such as single-ended or differential amplifiers could be improved by controlling the immittance they see. This is achieved by utilizing the proposed baluns in those situations. For a specific operating bandwidth and passband ripple, the commensurate frequency of the presented baluns can be varied, resulting in a wide range of terminal immittance values. Additional tapping of the balanced resonators of the baluns leads to the realization of specific balanced-to-single-ended immittance ratios at no increase in overall size. Two baluns were designed using a synthesis procedure. Measured and simulated specifications were in close agreement.

APPENDIX I

As described in [9], given the element values of the prototype depicted in Fig. 3(b), the following parameters must first be evaluated:

$$K = \sqrt{\frac{Z_{c3}}{Z_{c1} + Z_{c2} + Z_{c3}}} \tag{20}$$

$$Z_a = \frac{Z_{c1}}{\sqrt{1 - K^2}} \tag{21}$$

$$Z_b = \frac{Z_{c2}}{\sqrt{1 - K^2}}. \tag{22}$$

Using the above equations, the modal impedances of each individual coupled-line pair comprising the balun shown in Fig. 3(a) are found as follows:

$$Z_{\text{oea}} = Z_a \sqrt{\frac{1 + K_a}{1 - K_a}} \text{ and } Z_{\text{ooa}} = \frac{Z_a^2}{Z_{\text{oea}}} \tag{23}$$

$$Z_{\text{oeb}} = Z_b \sqrt{\frac{1 + K_b}{1 - K_b}} \text{ and } Z_{\text{oob}} = \frac{Z_b^2}{Z_{\text{oeb}}} \tag{24}$$

where $K_a = K_b = K$. The characteristic impedances of the open-circuited stub Z_{oc4} and the balanced load R_B are then determined using

$$Z_{\text{oc4}} = Z_{c4}/K^2 \quad R_B = R_{\text{oB}}/K^2. \tag{25}$$

Finally, the characteristic impedances of all of the remaining stubs in Fig. 3(a) are then found from

$$Z_{\text{oc1}} = Z_{o1}, Z_{\text{oc2}} = Z_{o3} \text{ and } Z_{\text{oc3}} = Z_{o2}. \tag{26}$$

REFERENCES

[1] R. Mongia, I. Bahl, and P. Bhartia, *RF and Microwave Coupled-Line Circuits*. Norwood, MA: Artech House, 1999, pp. 411–435.

[2] I. D. Robertson and S. Lucyszyn, "RFIC and MMIC design and technology," *Proc. Inst. Elect. Eng.—Circuits, Devices Syst.*, ser. 13, pp. 281–346, 2001.

[3] B. J. Minnis and M. Healy, "New broadband balun structures for monolithic microwave integrated circuits," in *IEEE MTT-S Int. Microw. Symp. Dig.*, Jun. 1991, pp. 425–428.

[4] A. M. Pavio and A. Kikel, "A monolithic or hybrid broad-band compensated balun," in *IEEE MTT-S Int. Microw. Symp. Dig.*, May 1990, pp. 483–486.

[5] D. Kuylenstierna and P. Linner, "Design of broad-band lumped-element baluns with inherent impedance transformation," *IEEE Trans. Microw. Theory Tech.*, vol. 52, no. 12, pp. 2739–2745, Dec. 2004.

[6] N. Marchand, "Transmission line conversion transformers," *Electron.*, vol. 17, no. 12, pp. 142–145, Dec. 1944.

[7] J. Cloete, "Graphs of circuit elements for the Marchand balun," *Microw. J.*, vol. 24, no. 5, pp. 125–128, May 1981.

[8] C. L. Goldsmith, A. Kikel, and N. L. Wilkens, "Synthesis of Marchand baluns using multilayer microstrip structures," *Int. J. Microw. Millimeter-Wave Comput.-Aided Eng.*, vol. 2, no. 3, pp. 179–188, 1992.

[9] W. M. Fathelbab and M. B. Steer, "New classes of miniaturized planar Marchand baluns," *IEEE Trans. Microw. Theory Tech.*, vol. 53, no. 4, pp. 1211–1220, Apr. 2005.

[10] K. Nishikawa, I. Toyoda, and T. Tokumitsu, "Compact and broad-band three-dimensional MMIC balun," *IEEE Trans. Microw. Theory Tech.*, vol. 47, no. 1, pp. 96–98, Jan. 1999.

[11] C. Tsai and K. C. Gupta, "A generalized model for coupled lines and its applications to two-layer planar circuits," *IEEE Trans. Microw. Theory Tech.*, vol. 40, no. 12, pp. 2190–2199, Dec. 1992.

[12] C. W. Tang and C. Y. Chang, "A semi-lumped balun fabricated by low temperature co-fired ceramic," in *IEEE MTT-S Int. Microw. Symp. Dig.*, Jun. 2002, pp. 2201–2204.

[13] K. S. Ang, Y. C. Leong, and C. H. Lee, "Analysis and design of miniaturized lumped-distributed impedance-transforming baluns," *IEEE Trans. Microw. Theory Tech.*, vol. 51, no. 3, pp. 1009–1017, Mar. 2003.

[14] R. J. Wenzel, "Application of exact synthesis methods to multi-channel filter design," *IEEE Trans. Microw. Theory Tech.*, vol. MTT-13, no. 1, pp. 5–15, Jan. 1965.

[15] R. Levy, "Synthesis of general asymmetric singly and doubly terminated cross-coupled filters," *IEEE Trans. Microw. Theory Tech.*, vol. 42, no. 12, pp. 2468–2471, Dec. 1994.

[16] B. J. Minnis, *Designing Microwave Circuits by Exact Synthesis*. Norwood, MA: Artech House, 1996.

[17] H. J. Carlin and P. P. Civalleri, *Wideband Circuit Design*. Boca Raton, FL: CRC, 1998.

[18] E. Cristal, "Tapped-line coupled transmission lines with applications to interdigital and combline filters," *IEEE Trans. Microw. Theory Tech.*, vol. MTT-23, no. 12, pp. 1007–1012, Dec. 1975.

[19] M. Horton and R. Wenzel, "General theory and design of optimum quarter-wave TEM filters," *IEEE Trans. Microw. Theory Tech.*, vol. MTT-13, no. 5, pp. 316–327, May 1965.

[20] J. A. G. Malherbe, *Microwave Transmission Line Filters*. Norwood, MA: Artech House, 1979.

[21] J. A. G. Malherbe, "Realization of elliptic function bandstop filters by means of resonated prototype," *IEEE Trans. Microw. Theory Tech.*, vol. MTT-25, no. 8, p. 717, Aug. 1977.

[22] Advanced Design System (ADS). ver. 2003A, Agilent Technol., Palo Alto, CA, 2003.

Wael M. Fathelbab (M'03–SM'05) received the B.Eng. and Ph.D. degrees from the University of Bradford, Bradford, U.K., in 1995 and 1999, respectively.

From 1999 to 2001, he was an RF Engineer with Filtronic Comtek Ltd., where he was involved in the design and development of filters and multiplexers for various cellular base-station applications. He was subsequently involved with the design of novel RF front-end transceivers for the U.K. market with the Mobile Handset Division, NEC Technologies Ltd. He is currently a Research Associate with the Department of Electrical and Computer Engineering, North Carolina State University, Raleigh. His research interests include network synthesis techniques, the design of tunable microwave devices, and broadband matching theory. He will be joining the Department of Electrical and Computer Engineering, South Dakota School of Mines and Technology, Rapid City, as an Assistant Professor in August 2006.

Michael B. Steer (S'76–M'82–SM'90–F'99) received the B.E. and Ph.D. degrees in electrical engineering from the University of Queensland, Brisbane, Australia, in 1976 and 1983, respectively.

He is currently the Lampe Family Distinguished Professor of Electrical and Computer Engineering, North Carolina State University, Raleigh. In 1999 and 2000, he was a Professor with the School of Electronic and Electrical Engineering, The University of Leeds, where he held the Chair in microwave and millimeter-wave electronics. He was also Director of the Institute of Microwaves and Photonics, The University of Leeds. He has authored approximately 300 publications on topics related to RF, microwave and millimeter-wave systems, high-speed digital design, and RF and microwave design methodology and circuit simulation. He coauthored *Foundations of Interconnect and Microstrip Design* (Wiley, 2000).

Prof. Steer is active in the IEEE Microwave Theory and Techniques Society (IEEE MTT-S). In 1997, he was secretary of the IEEE MTT-S. From 1998 to 2000, he was an elected member of its Administrative Committee. He is the Editor-in-Chief of the IEEE TRANSACTIONS ON MICROWAVE THEORY AND TECHNIQUES (2003–2006). He was a 1987 Presidential Young Investigator (USA). In 1994 and 1996, he was the recipient of the Bronze Medallion presented by the Army Research Office for "Outstanding Scientific Accomplishment." He was also the recipient of the 2003 Alcoa Foundation Distinguished Research Award presented by North Carolina State University.